^{31}P NMR as a Tool for Studying Incorporation of Ni, Co, Fe, and Mn into Aluminophosphate Zeotypes

Gregor Mali,*,† Alenka Ristić,† and Venčeslav Kaučič†,‡

National Institute of Chemistry, Hajdrihova 19, SI-1001 Ljubljana, Slovenia, and University of Ljubljana, SI-1000 Ljubljana, Slovenia

Received: January 20, 2005; In Final Form: March 25, 2005

The incorporation of moderate amounts of Ni(II), Co(II), Fe(II/III), and Mn(II/III) into aluminophosphate zeotype $AlPO_4$-34 and Fe(II/III) into aluminophosphate zeotype $AlPO_4$-36 was studied by broadline ^{31}P NMR. The technique provided direct evidence on isomorphous substitution of framework aluminum by transition metals and allowed us to determine the extent of the substitution. ^{31}P NMR proved to be complementary to other spectroscopic techniques such as X-ray absorption spectroscopy (XAS), Mössbauer, electron paramagnetic resonance (EPR), and electron nuclear double resonance (ENDOR) spectroscopies. The position of the NMR signal belonging to phosphorus in the $P(OAl)_3(OMe)$ environment depended mostly on the magnitude of the hyperfine interaction between a phosphorus nucleus and an unpaired electron, which was delocalized from the transition metal atom Me by covalent bonding. The width of the NMR signal was dominated by dipolar coupling among phosphorus nuclei and nearest paramagnetic centers. In addition, broadline NMR of ethylenediamine-templated manganese phosphate $(C_2H_{10}N_2)[Mn_2(HPO_4)_3(H_2O)]$, which was used as a model compund, showed that on the basis of line positions and line widths different ^{31}P signals could easily be assigned to different phosphorus crystallographic sites. The technique could thus be applied to extract valuable structural information about metal phosphates as well.

Introduction

Aluminophosphate molecular sieves[1] ($AlPO_4$-*n*, where *n* denotes a specific structure type) form a family of synthetic zeolite-like materials with a large number of distinct three-dimensional microporous structures.[2,3] Unlike in typical zeolites, frameworks of aluminophosphate molecular sieves are electrically neutral and thus exhibit no ion-exchange ability or acidity. Modification of such frameworks with heteroatoms,[4] particularly with transition metal ions, however, introduces catalytic properties to these materials; substitution of divalent transition metal ions for trivalent aluminum imparts charge imbalance, which results in a solid acid catalyst when compensated by a proton. Furthermore, through their ability to change oxidation state upon heating in an oxygen or hydrogen atmosphere, transition metal ions introduce redox properties to aluminophosphate materials. The interplay among the transition metal redox properties, the presence of framework acid centers, and the unique pore architecture makes the preparation of modified aluminophosphate molecular sieves ($MeAlPO_4$-*n* materials) an important discipline in the design of new catalysts.[5]

A prerequisite for understanding the catalytic properties of MeAlPOs is a thorough characterization of the transition metal ion environment. Over the years, infrared, UV−vis, electron paramagnetic resonance (EPR), extended-X-ray absorption fine structure (EXAFS), and Mössbauer spectroscopies have been routinely applied for studying transition metal ions in aluminophosphates.[5] EXAFS provides a description of the short-range order in terms of the number of nearest neighbors to the transition metal ion and distances to these neighbors. EPR is best suited for characterizing systems with low levels of paramagnetic transition metal ions, but its information content is usually limited to the identification of the paramagnetic species present in the sample and of the local symmetry of paramagnetic sites. Mössbauer spectroscopy was used less in characterization of modified aluminophosphates, because it is limited to those elements that exhibit the Mössbauer effect. Thus, it provided valuable information on oxidation states, magnetic fields, and lattice symmetry of heteroatom sites in iron-, tin-, and indium-containing aluminophosphates.

Better insight into the chemical environment of transition metal ions and direct evidence for the isomorphous framework substitution could be provided by spectroscopic techniques that not only yield information on coordination with nearest oxygen atoms but also detect hyperfine interactions with neighboring aluminum or phosphorus nuclei. Electron spin−echo envelope modulation (ESEEM) and electron nuclear double resonance (ENDOR) are two such techniques, of which the latter one was recently used for studying several Mn(II)-containing aluminophosphate molecular sieves.[6−9] The detection of ^{31}P hyperfine couplings in the range 5−8 MHz and the absence of such ^{27}Al interaction served as combined proof for isomorphous substitution of Mn(II) for Al. Hyperfine couplings between unpaired electrons from paramagnetic Co(II/III) ions and framework ^{31}P nuclei were also detected by broadline ^{31}P NMR in several cobalt-containing aluminophosphates.[10,11] The phosphorus signals due to ^{31}P in $P(OAl)_{4-n}(OCo)_n$ environments were typically shifted by about $n \times 2250$ ppm relative to the signal of ^{31}P in the $P(OAl)_4$ environment, and this large shift was attributed to electron−nucleus hyperfine coupling. Broadline ^{31}P NMR spectra enabled authors to also determine the amount of Co incorporated into framework aluminum positions and to describe the distribution of Co within the lattice.

* e-mail address: gregor.mali@ki.si.
† National Institute of Chemistry.
‡ University of Ljubljana.

10.1021/jp050358n CCC: $30.25
Published on Web 05/11/2005

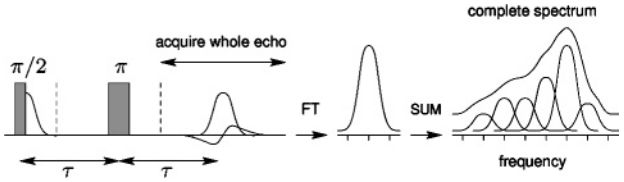

Figure 1. Schematic representation of the spin−echo mapping technique used for recording broad phosphorus NMR spectra. Vertical dashed lines mark instrumental dead time after each radio frequency pulse.

TABLE 1: Elemental Composition of Selected As-Synthesized MeAlPO$_4$-*n* Materials and Oxidation State and Coordination of Transition Metal Ions in As-Synthesized and Calcined Rehydrated Samples[a]

	composition	as-synthesized	calcined rehydrated
NiAlPO$_4$−34	$Ni_{0.04}Al_{0.95}PO_4$	tetrahedral, 2+	tetrahedral, 2+
CoAlPO$_4$−34	$Co_{0.05}Al_{0.95}PO_4$	tetrahedral, 2+	tetrahedral, 2+
FeAlPO$_4$−34	$Fe_{0.05}Al_{0.92}PO_4$	octahedral, 2+/3+	octahedral, 3+
MnAlPO$_4$−34	$Mn_{0.05}Al_{0.96}PO_4$	tetrahedral, 2+	octahedral, 3+
FeAlPO$_4$−36	$Fe_{0.08}Al_{0.92}PO_4$	octahedral, 2+/3+	octahedral, 3+

[a] Summarized from refs 13, 14, and 15.

In this contribution, we shall show that broadline ^{31}P NMR can be employed for studying Ni, Fe, and Mn incorporation as well. In contrast to ENDOR spectroscopy, which works best if the extent of substitution is very small (Me/Al fraction below 1%), ^{31}P NMR proves to be better suited for analyzing materials with a moderate or large fraction of incorporated transition metal (Me/Al fraction above 1%). We shall discuss the ^{31}P NMR line position and line width and try to relate them to the magnitude of hyperfine and dipolar couplings between unpaired transition metal electrons and phosphorus nuclei.

Materials and Methods

Nickel-, cobalt-, iron-, and manganese-containing MeAlPO$_4$-34 aluminophosphate molecular sieves were prepared hydrothermally in a fluoride medium. Details of the synthesis were described in refs 12 and 13. MeAlPO$_4$-34 materials have chabazite topology with 8-membered pore openings of the diameter 0.38 nm and thus belong to so-called small-pore microporous materials. The FeAlPO$_4$-36 zeotype was prepared hydrothermally as described in ref 14. The material exhibits a one-dimensional system of channels formed by elliptical 12-membered rings with dimensions of 0.74 nm × 0.65 nm. If side pockets inside the channel opened, the dimensions of the channel's cross-section would enlarge to 1.01 nm × 0.92 nm. FeAlPO$_4$-36 belongs to large-pore microporous materials. The oxidation state and local symmetry of transition metal ions in all as-synthesized and calcined rehydrated materials were determined by XANES and EXAFS measurements. Results of these measurements are summarized in Table 1 along with the elemental composition of MeAlPOs. Manganese phosphate templated by ethylenediamine $(C_2H_{10}N_2)[Mn_2(HPO_4)_3(H_2O)]$ was synthesized hydrothermally as described in ref 16.

Broadline ^{31}P NMR spectra of as-synthesized and calcined rehydrated MeAlPOs were recorded by the spin−echo mapping[11,17] (or variable offset cumulative spectroscopy[18]) technique. Schematically, the method consists of recording a series of spectra using the Hahn echo sequence at different irradiation frequencies (Figure 1). For each spectrum, the intensity is corrected, taking into account the relaxation of the magnetization before acquisition of the signal. The total signal is obtained by the addition of all individual spectra. Under specific conditions, the spectrum obtained by spin−echo mapping can reproduce the real line shape. All NMR measurements were carried out on a Varian Unity Plus 300 spectrometer, operating at a ^{31}P Larmor frequency of 122.65 MHz. The width of $\pi/2$ pulses was 2.5 μs, and the separation τ between the $\pi/2$ and π pulses was 20 μs. The irradiation frequency was incremented in 100-kHz steps, and the number of increments was dictated by the frequency limits beyond which the NMR signal was negligible. In all spectra, the frequency difference ($\Delta\nu = \nu - \nu_0$) relative to the Larmor frequency (ν_0) of phosphorus nuclei within an 85% solution of H_3PO_4 is reported.

Theoretical Basis. As already mentioned, the ^{31}P NMR spectrum is affected by paramagnetic transition metal ions because of strong dipolar and hyperfine interactions of unpaired electrons with phosphorus nuclei. The influence of a single paramagnetic center can be expressed through an effective magnetic field of the form[19]

$$B_{en} = \frac{2\pi A_{iso}}{\gamma_n}\langle S\rangle + \mu_0\mu_B g\frac{3\cos^2\theta - 1}{r^3}\langle S\rangle \qquad (1)$$

where A_{iso} is the isotropic hyperfine coupling constant, γ_n is the nuclear gyromagnetic ratio, μ_B is the Bohr magneton, r is the separation between the electronic and nuclear spins, and θ is the angle between the electron−nucleus vector and the external magnetic field. Note that the nucleus experiences the interaction with a single paramagnetic center only in samples with low fractions of homogeneously distributed transition metal ions. In samples with a higher fraction of transition metal ions, the contribution of several paramagnetic centers should be considered. Rapid electron spin relaxation is assumed in the above expression; therefore, the electron spin quantum number can be replaced with the average electron spin polarization $\langle S\rangle$, which is described as

$$\langle S\rangle = \frac{\mu_B g B_0 S(S+1)}{3kT} \qquad (2)$$

The first term in eq 1 comes from the hyperfine coupling and is responsible for isotropic shift of ^{31}P NMR lines. The second term in eq 1 comes from the electron−nucleus dipolar coupling. It has angular dependence and thus causes broadening of the ^{31}P NMR lines in powders. The angular dependence of the electron−nucleus dipolar coupling is equivalent to the angular dependence of axially symmetric chemical shift anisotropy, although the magnitude in modified aluminophosphate molecular sieves will turn out to be much larger. The description of the electron−nucleus dipolar coupling should actually take into account that electronic spin is delocalized from the transition metal and can be found with substantial probability at least on surrounding oxygen ions. However, even though a sum of dipolar contributions over all such sites was considered and even though anisotropic g tensors were considered instead of their isotropic values, the shape of the powder pattern induced by this interaction would still resemble the shape of the powder pattern induced by the chemical shift anisotropy.[19,20] It is worth noting that both terms in eq 1 depend on averaged electron spin polarization $\langle S\rangle$. This means that a transition metal ion with a larger spin quantum number S will induce larger NMR line broadening and, if A_{iso} was fixed, a larger paramagnetic shift.

Arieli and co-workers recently performed ENDOR spectroscopy on MnAlPO$_4$-20, MnAlPO$_4$-5, and MnAlPO$_4$-11 microporous molecular sieves and determined the isotropic hyperfine coupling constant for ^{31}P to be about 8 MHz.[7] By taking this value for an estimate of A_{iso} and by choosing some typical values

TABLE 2: Theoretical Estimation of ^{31}P NMR Linewidths and Paramagnetic Shifts Due to the Interaction with Different Transition Metal Ions[a]

ion	configuration	S	width[b]/kHz	shift[c]/kHz
Mn(III)	d^4	2	600	480
Mn(II)/Fe(III)	d^5	$^5/_2$	875	700
Fe(II)/Co(III)	d^6	2	600	480
Co(II)	d^7	$^3/_2$	375	300
Ni(II)	d^8	1	200	160

[a] Obtained using eq 1. [b] Using $g = 2$, $B_0 = 7$ T, and $r = 0.34$ nm. [c] Using $A_{iso} = 8$ MHz.

for g, B_0, and r, we can use eqs 1 and 2 to estimate the width and the paramagnetic shift of lines in ^{31}P NMR spectra of different MeAlPO$_4$-n materials. The calculated values are gathered in Table 2. For all electronic configurations of transition metal ions listed in the table, the high-spin state was assumed. We notice that in an external magnetic field of 7 T the roughly estimated NMR line width is comparable to the isotropic paramagnetic shift of the line and that they both can reach nearly megahertz range. Note, however, that the calculated shifts offer only very rough estimation, because hyperfine coupling is probably not equally strong for different transition metals. Indeed, the isotropic hyperfine coupling in FeAlPO$_4$-20 determined by ENDOR was about 20% weaker than the coupling in MnAlPO$_4$-20.[7] Relations between line widths are also only suggestive. The estimation predicts, for example, that the width of the ^{31}P NMR line should increase by a factor of 1.5 upon oxidation of Fe(II) to Fe(III) or upon reduction of Mn(III) to Mn(II). The prediction, however, does not take into account changes in the distribution of unpaired electrons and changes in electron−nuclear distances.

Results and Discussion

The sum of a series of narrow spectra recorded at different irradiation frequencies yields a proper broadline ^{31}P NMR spectrum only if the individual contributions are correctly weighted, that is, if the loss in their intensities due to transverse relaxation is properly compensated for. Obviously, correcting the spectra requires careful relaxation measurements at each irradiation frequency. Results of such measurements for a series of MeAlPO$_4$-34 molecular sieves are shown in Figure 2a. Transverse relaxation is much slower for phosphorus nuclei within the P(OAl)$_4$ environment ($\Delta\nu \approx 0$) than for phosphorus nuclei within the P(OAl)$_3$(OMe) environment ($\Delta\nu > 100$ kHz). For the latter, moreover, the relaxation rate increases with the irradiation frequency, which means that signals that exhibit larger shifts relax more rapidly and are thus more difficult to detect and accurately quantify. The problem with proper compensation of losses due to fast relaxation is illustrated in Figure 2b,c. Whereas slow relaxation of a signal of NiAlPO$_4$-34 at $\Delta\nu = 0$ allows one to describe the relaxation curve unequivocally by a Gaussian function, fast relaxation of a signal at $\Delta\nu = 600$ kHz accompanied by the absence of initial data points due to instrumental dead time limitations and of final data points due to signal-to-noise limitations leads to almost equally good descriptions of the relaxation curve with either Gaussian or exponential functions. The two curves, however, provide different zero-time intensities (i.e., different correction factors for the intensity of a spectrum recorded at $\Delta\nu$ of 600 kHz). This ambiguity in the magnitude of correction factors, especially for high-frequency parts of the signal, sets the limits in accuracy of the determination of the amount of transition metal occupying framework aluminum sites within MeAlPO$_4$-34 and FeAlPO$_4$-36 materials.

Corrected broadline ^{31}P NMR spectra of as-synthesized and calcined rehydrated samples of AlPO$_4$-34, NiAlPO$_4$-34, CoAlPO$_4$-34, FeAlPO$_4$-34, MnAlPO$_4$-34, and FeAlPO$_4$-36 molecular sieves are shown in Figure 3. Magic angle spinning spectra of both pure AlPO$_4$-34 samples are shown as well, demonstrating that in the as-synthesized sample three inequivalent phosphorus signals can be resolved, corresponding to three inequivalent phosphorus crystallographic sites.[21] Within the calcined rehydrated sample, there are six inequivalent phosphorus sites,[22] but they cannot be resolved in a spectrum recorded at 7 T. In static spectra of both samples, signals of phosphorus nuclei from different crystallographic sites overlap extensively and constitute a single, approximately 5-kHz-wide line.

Whereas for pure AlPO$_4$-34 samples only strong signals belonging to ^{31}P nuclei within a P(OAl)$_4$ environment can be observed, spectra of modified MeAlPOs also exhibit broad signals with lower peak heights shifted to higher frequencies by several hundred kilohertz. A single exception is the spectrum of the as-synthesized MnAlPO$_4$-34 sample. We shall discuss possible reasons for the absence of an additional broad contribution to the phosphorus spectrum of this sample later. The presence of the broad shifted signal is a consequence of the combined hyperfine and dipolar interaction of phosphorus nuclei with transition metal ions and is thus a direct proof for the isomorphous substitution of part of the framework aluminum with transition metals. To the best of our knowledge, this is the first evidence for the incorporation of Ni, Fe, and Mn into the aluminophosphate framework obtained by broadline ^{31}P NMR.

The spectra not only detect the interaction between phosphorus nuclei and transition metal ions but also enable one to determine the amount of transition metal occupying framework aluminum positions. In a MeAlPO$_4$-34 sample with homogeneously distributed transition metal ions, the signal belonging to P(OAl)$_{4-n}$(OMe)$_n$ groups contributes

$$\binom{4}{n} p^n (1-p)^{4-n} \tag{3}$$

to the total phosphorus signal. Here, p and $(1-p)$ denote Me/P and Al/P fractions, respectively, and assume that Me/P + Al/P = 1. For $p \approx 5\%$ (see Table 1), phosphorus nuclei from P(OAl)$_4$, P(OAl)$_3$(OMe), and P(OAl)$_2$(OMe)$_2$ groups should thus contribute approximately 81%, 17%, and 1% to the total NMR signal. Obviously, the contribution of phosphorus nuclei that interact with more than one transition metal ion can safely be neglected. On the basis of eq 3, one can easily analyze phosphorus NMR spectra and use the relative contribution of the P(OAl)$_4$ signal to experimentally determine the Me/P fraction. Results of such quantitative analyses on MeAlPO$_4$-34 and FeAlPO$_4$-36 samples are collected in Table 3. We can see that Me/P fractions determined by broadline ^{31}P NMR mostly agree well with results of the elemental analysis. Noticeable exceptions are only very small amounts of Fe(III) detected within calcined rehydrated FeAlPO$_4$-34 and FeAlPO$_4$-36. According to elemental analysis, these amounts should reach about 80% of the values found for the as-synthesized materials. A possible reason for the discrepancy between the results of the NMR and the elemental analysis is that part of the iron leached out of the framework during calcination and remained trapped within cavities. Such iron would only be detected by elemental analysis and not by ^{31}P NMR spectroscopy. The possibility of leaching and the presence of extraframework iron were mentioned already in ref 23. The overall accuracy of the measurement could be improved if more reliable relaxation analysis

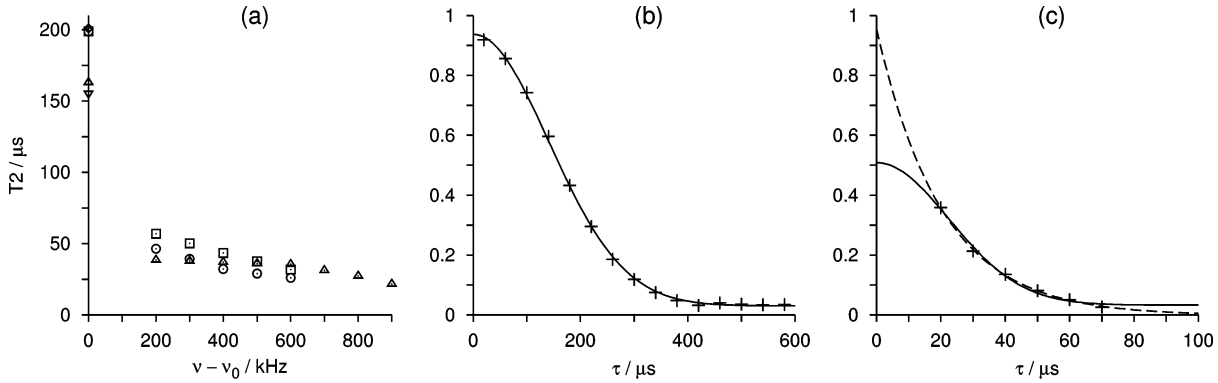

Figure 2. Transverse relaxation in selected $MeAlPO_4$-34 materials. (a) Transverse phosphorus relaxation time T_2 as a function of the irradiation frequency in as-synthesized samples of $AlPO_4$-34 (◇), $NiAlPO_4$-34 (□), $CoAlPO_4$-34 (○), $FeAlPO_4$-34 (△), and $MnAlPO_4$-34 (▽). T_2 was determined by fitting a Gaussian function to relaxation curves obtained by varying the separation between two pulses in the Hahn echo pulse sequence. (b) and (c) show relaxation curves recorded in $NiAlPO_4$-34 at $\Delta\nu$ of 0 and 600 kHz, respectively. Solid lines in (b) and (c) show best-fit Gaussian curves, and dashed line in (c) shows best-fit exponential curve.

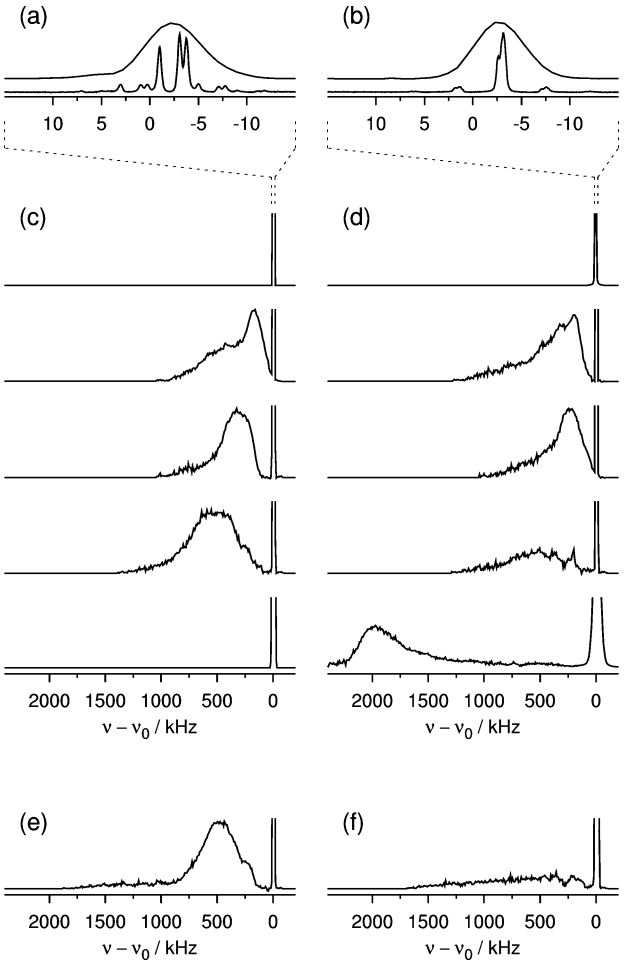

Figure 3. Broadline ^{31}P NMR in several as-synthesized and calcined rehydrated $MeAlPO_4$-34 and $FeAlPO_4$-36 molecular sieves. (a) and (b) show ^{31}P static and magic angle spinning (MAS) NMR spectra in a narrow region around ν_0. In (c), static spectra of as-synthesized samples of $AlPO_4$-34, $NiAlPO_4$-34, $CoAlPO_4$-34, $FeAlPO_4$-34, and $MnAlPO_4$-34 follow from top to bottom. In (d), the corresponding spectra of calcined rehydrated samples are shown. In (e) and (f), the spectra of the as-synthesized and calcined rehydrated samples of $FeAlPO_4$-36 are shown, respectively.

could be performed, and thus, more accurate spectra and intensities following from them were obtained. In contrast to elemental analysis that is usually carried out on only a few crystallites whose elemental composition can vary significantly, the determination of the Me/P fraction by NMR is truly a bulk

TABLE 3: Me/P Fraction (in %) of Selected As-Synthesized and Calcined Rehydrated $MeAlPO_4$-*n* Materials as Determined by Broadline ^{31}P NMR Measurements

	as-synthesized	calcined rehydrated
$NiAlPO_4-34$	5.0 ± 0.7	5.0 ± 0.9
$CoAlPO_4-34$	3.9 ± 1.0	3.8 ± 0.7
$FeAlPO_4-34$	5.7 ± 2.0	2.7 ± 1.0
$MnAlPO_4-34$		7.0 ± 2.9
$FeAlPO_4-36$	9.0 ± 2.4	1.8 ± 0.7

method working on a large amount of material and thus providing reliable powder averaging. Furthermore, the fraction determined by NMR really reflects the amount of transition metal occupying framework aluminum sites and does not consider transition metal trapped within cavities. On the other hand, it also does not detect transition metal ions that might be located on phosphorus instead of aluminum sites. The detection limits of broadline ^{31}P NMR spectroscopy depend on the transition metal incorporated into the aluminophosphate framework. Narrower signals that relax more slowly are easier to detect than very broad and rapidly relaxing ones. Inspecting the spectra presented in Figure 3, we assume that Me/P fractions down to about 1% could readily be detected in Ni(II)-, Co(II)-, or Fe(II)-modified aluminophosphate molecular sieves.

Despite theoretical predictions, line shapes of $P(OAl)_3(OMe)$ signals in ^{31}P NMR spectra of $MeAlPO_4$-*n* materials do not resemble chemical shift anisotropy (CSA) powder patterns. This is most probably due to the overlap of a number of slightly different and slightly displaced CSA-like signals belonging to phosphorus nuclei that occupy several crystallographically distinct sites and experience interaction with transition metal ions sitting on several different framework positions as well. Such distribution and overlap of signals make the comparison between the detected and theoretically predicted NMR line widths and paramagnetic shifts more difficult. Nevertheless, spectra recorded in the as-synthesized samples of $NiAlPO_4$-34, $CoAlPO_4$-34, and $FeAlPO_4$-34 do reflect the predicted dependency on the spin quantum number *S*. Peak position frequencies of 170, 300, and 500 kHz for Ni-, Co-, and $FeAlPO_4$-34, respectively, and full widths at half-maximum (fwhm's) of 300 and 500 kHz for Co- and $FeAlPO_4$-34, respectively, agree well with roughly estimated values that were given in Table 2. In the as-synthesized $FeAlPO_4$-36, the paramagnetic shift and line width of the $P(OAl)_3(OFe)$ signal are slightly smaller than in the as-synthesized $FeAlPO_4$-34. This is expected, because in large-pore microporous materials P−O−Al and P−O−Fe bond distances are generally larger than in small-pore microporous

materials and thus induce weaker dipolar and hyperfine couplings. For the latter coupling, the phenomenon was already detected by ENDOR spectroscopy of a series of Mn(II)-containing aluminophosphates, showing that the isotropic hyperfine coupling constant for phosphorus can range from about 8 MHz in microporous to about 5 MHz in mesoporous materials.[7]

Upon calcination and rehydration of samples, the spectra of $NiAlPO_4$-34 and $CoAlPO_4$-34 do not change appreciably, which is understandable, because the oxidation state and the symmetry of Ni and Co ions do not change either. Small changes are expected only because of the small framework distortion introduced by calcination and rehydration. Spectra of $FeAlPO_4$-34 and $FeAlPO_4$-36 exhibit broadening due to oxidation of Fe(II) ($S = 2$) to Fe(III) ($S = {}^5/_2$) and suggest the loss of some framework iron. The spectra of $MnAlPO_4$-34 samples are the most difficult to explain. The NMR signal of the phosphorus nuclei experiencing interaction with paramagnetic Mn(III) ions of the calcined rehydrated sample is shifted much more than signals in other $MeAlPO_4$-*n* materials. Bonding of phosphorus nuclei to more than one Mn ion could induce that large paramagnetic shift, but clustering of manganese was not suggested by quantitative analysis of $P(OAl)_{4-n}(OMn)_n$ signals. Another possibility is extremely strong phosphorus-to-manganese hyperfine coupling exceeding that between phosphorus and iron by a factor of 3 or 4. ENDOR spectroscopy of $MnAlPO_4$-34 might elucidate this problem.

On the other hand, a large shift in the ^{31}P NMR spectrum of the calcined rehydrated $MeAlPO_4$-34 aids in the explanation of the NMR spectrum of its as-synthesized form. A quantitative comparison of phosphorus spectra of pure and Mn-modified $AlPO_4$-34 molecular sieves suggests that more than 20% of phosphorus in the as-synthesized $MnAlPO_4$-34 is "NMR invisible". It seems that phosphorus nuclei within $P(OAl)_{4-n}(OMn)_n$ groups with $n \geq 1$ are exposed to extremely strong interaction with Mn(II) ions. If Mn(III) ions ($S = 2$) induce surprisingly large paramagnetic shifts, Mn(II) ions with even higher spin quantum number ($S = {}^5/_2$) are expected to displace and broaden phosphorus NMR signals even more severely. Such signals might be very difficult to detect with our current experimental setting and our current detection limits. Moreover, as shown in Figure 2, a larger shift is associated with faster relaxation, meaning that in the as-synthesized $MnAlPO_4$-34 transverse phosphorus magnetization of $P(OAl)_3(OMn)$ groups could decay even before the spin−echo was actually formed, thus leading to nuclei truly invisible by the proposed NMR method.

To demonstrate that Mn(II) is not necessarily a problematic ion for broadline ^{31}P NMR spectroscopy and that better defined line shapes can indeed be obtained if distribution and overlap of many contributions is avoided, we recorded a spectrum of manganese phosphate templated by ethylenediamine ($C_2H_{10}N_2$)-[$Mn_2(HPO_4)_3(H_2O)$]. The material consists of anionic sheets constructed by edge-sharing MnO_6 octahedra and MnO_5 trigonal bipyramids, as well as hydrogen phosphate tetrahedra. The structure[24] is schematically presented in Figure 4a and the corresponding experimental and decomposed ^{31}P NMR spectra are shown in Figure 4b,c, respectively. The spectrum can be decomposed into three equally intense lines: two of them can be described well by Gaussian shape, and the third one can be excellently fit by a line shape resembling axially symmetric chemical shift anisotropy. Realizing that $P(1)O_3(OH)$ and $P(3)O_3(OH)$ tetrahedra are nearly equivalent, both sharing a corner common to $Mn(2)O_6$ and $Mn(3)O_6$ octahedra and a corner with $Mn(1)O_5$ bipyramid, it is not difficult to assign the broad and displaced CSA-like line to the P2 site. Moreover, the large width and paramagnetic shift of its NMR line can be consistently explained by local surrounding of this site. A $P(2)O_3(OH)$ tetrahedron shares a corner common to $Mn(1)O_5$ and $Mn(2)O_6$ polyhedra, a corner common to $Mn(1)O_5$ and $Mn(3)O_6$ polyhedra, and a corner with $Mn(1)O_5$ bipyramid. P2 nuclei thus experience much larger dipolar and hyperfine couplings than P1 and P3.

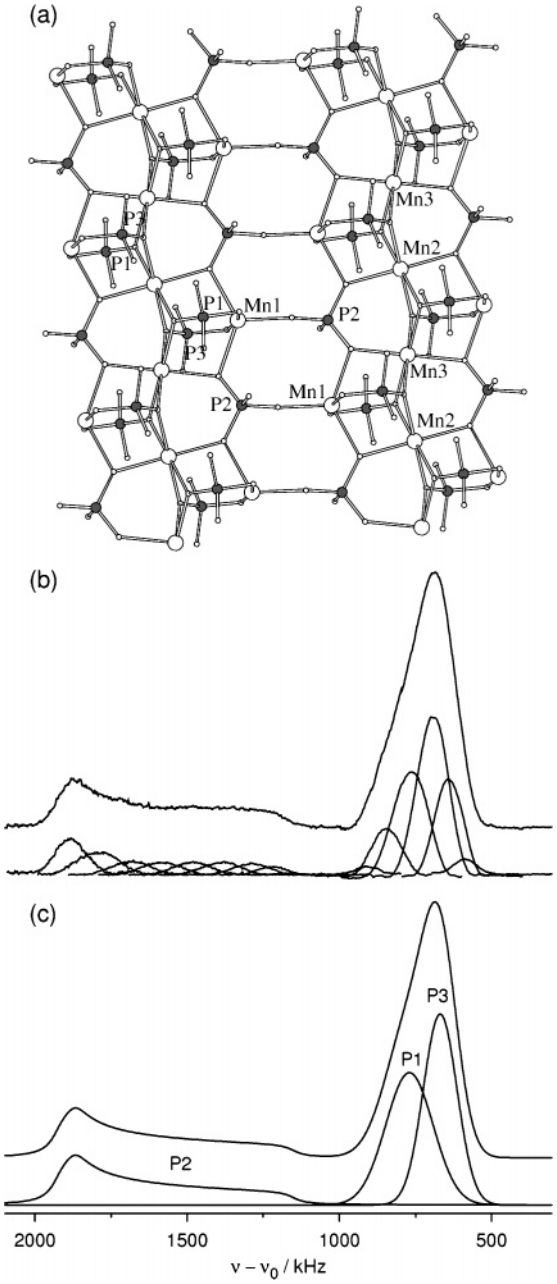

Figure 4. Broadline ^{31}P NMR of layered manganese phosphate. (a) Schematic representation of connectivities among three crystallographically distinct phosphorus and three crystallographically distinct manganese sites within a layer of manganese phosphate. Large open circles, filled circles, and small open circles represent Mn, P, and O sites, respectively. (b) Broadline ^{31}P NMR spectrum was obtained as a sum of a series of narrow spectra recorded at different irradiation frequencies. (c) Spectral decomposition with three equally intense lines, two Gaussian and one CSA-like. Individual lines are assigned to individual phosphorus crystallographic sites.

Assignment of two overlapped Gaussian lines to two distinct phosphorus sites can be accomplished by focusing on the fine structural differences between sites P1 and P3. As it was shown

recently, the magnitude of manganese-to-phosphorus hyperfine coupling depends on the total Mn−O−P bond length and on the corresponding bond angle. Shorter bonds and angles closer to 180° induce stronger hyperfine coupling.[7] Dipolar coupling between a phosphorus nucleus and a manganese ion depends not on bond length but on slightly different direct through-space Mn−P distances. Comparison of these three values for sites P1 and P3 shows that both average Mn−O−P bond length and average through-space Mn−P distance are shorter for the P1 site and also that the average Mn−O−P1 bond angle is closer to 180° than the average Mn−O−P3 bond angle is. All these values thus indicate that the phosphorus NMR signal belonging to P1 is broader and more shifted than the signal belonging to P3. Obviously, detailed structural differences are reflected in the broadline ^{31}P NMR spectrum of manganese phosphate.

Having well-defined NMR lines, we were able to determine individual isotropic shifts and, using eq 1, extract values of the isotropic hyperfine constant A_{iso} out of them. The magnitudes of A_{iso} for manganese-to-phosphorus interactions obtained in this way were 8.8, 18.9, and 7.7 MHz for P1, P2, and P3 phosphorus nuclei, respectively. Broadline ^{31}P NMR thus proved to be an alternative method to ENDOR spectroscopy, because it could detect hyperfine couplings in samples with moderate or large fractions of paramagnetic species. A similar investigation on a series of two- and three-dimensional iron phosphates is currently in progress as well.

Conclusions

Broadline ^{31}P NMR spectroscopy provided direct evidence of the incorporation of Ni(II), Co(II), Fe(II/III), and Mn(III) ions into the aluminum framework sites of $MeAlPO_4$-34 and $FeAlPO_4$-36 aluminophosphate molecular sieves. Quantitative analysis of NMR spectra yielded information about the distribution and about the amount of the incorporated transition metals within the bulk material. The accuracy of these quantitative measurements was limited by the accuracy of transverse relaxation analysis and was, in general, higher for transition metal ions that induce a smaller paramagnetic shift and smaller NMR line broadening. The lower detection limit was estimated to be at an Me/P fraction of about 1%. There is no upper limit, and the method, in principle, performs better in materials with a higher fraction of transition metal. Comparison of ^{31}P NMR spectra of the as-synthesized and calcined rehydrated $FeAlPO_4$-34 and $FeAlPO_4$-36 samples suggested that iron ions partially leach out of the framework during calcination.

The paramagnetic shift of $P(OAl)_3(OMe)$ phosphorus NMR lines depends on hyperfine coupling between phosphorus nuclei and transition metals. Whereas analysis of ^{31}P NMR spectra of $MeAlPO_4$-34 and $FeAlPO_4$-36 samples, in which individual contributions of several different phosphorus sites are severely overlapped, allowed only the estimation of isotropic hyperfine coupling constants, their values in the manganese phosphate material were precisely determined. The width of NMR lines provided some information about direct dipolar interaction between phosphorus nuclei and transition metal ions and enabled at least a qualitative analysis of distances. Because it detects interaction between transition metal ions and phosphorus nuclei, that is the interaction that extends beyond the first coordination shell, broadline ^{31}P NMR spectroscopy complements XAS and Mössbauer spectroscopy. It also complements ESEEM and ENDOR spectroscopy, because it allows the measurement of hyperfine coupling constants in metal phosphates and in MeAlPO materials with larger amounts of transition metals.

Acknowledgment. We thank Prof. Nevenka Rajić for providing Ni-containing samples and the Slovenian Ministry of Higher Education, Science and Technology for financial support through research projects P1-0021-0104 and J1-6350-0104-04.

References and Notes

(1) Wilson, S. T.; Lok, B. M.; Messina, C. A.; Cannan, T. R.; Flanigen, E. M. *J. Am. Chem. Soc.* **1982**, *104*, 1146.
(2) Szostak, R. *Handbook of Molecular Sieves*; Van Nostrand Reinhold: New York, 1992.
(3) Baerlocher, Ch.; Meier, W. M.; Olson, D. H. *Atlas of Zeolite Framework Types*, 5th revised ed.; Elsevier: Amsterdam, 2001.
(4) Flanigen, E. M.; Lok, B. M.; Patton, R. L.; Wilson, S. T. *Pure Appl. Chem.* **1986**, *58*, 1351.
(5) Hartmann, M.; Kevan, L. *Res. Chem. Intermed.* **2002**, *28*, 625.
(6) Arieli, D.; Vaughan, D. E. W.; Strohmaier, K. G.; Goldfarb, D. *J. Am. Chem. Soc.* **1999**, *121*, 6028.
(7) Arieli, D.; Strohmaier, K. G.; Vaughan, D. E. W.; Goldfarb, D. *J. Phys. Chem. B* **2002**, *106*, 7509.
(8) Arieli, D.; Dealabie, A.; Groothaert, M.; Pierloot, K.; Goldfarb, D. *J. Phys. Chem. B* **2002**, *106*, 9086.
(9) Arieli, D.; Prisner, T. F.; Hertel, M.; Goldfarb, D. *Phys. Chem. Chem. Phys.* **2004**, *6*, 172.
(10) Canesson, L.; Tuel, A. *Chem. Commun.* **1997**, 241.
(11) Canesson, L.; Boudeville, Y.; Tuel, A. *J. Am. Chem. Soc.* **1997**, *119*, 10754.
(12) Rajić, N.; Ristić, A.; Tuel, A.; Kaučič, V. *Zeolites* **1997**, *18*, 115.
(13) Ristić, A.; Novak Tušar, N.; Arčon, I.; Thibault-Starzyk, F.; Hanžel, D.; Czyzniewska, J.; Kaučič, V. *Microporous Mesoporous Mater.* **2002**, *56*, 303.
(14) Ristić, A.; Novak Tušar, N.; Arčon, I.; Zabukovec Logar, N.; Thibault-Starzyk, F.; Czyzniewska, J.; Kaučič, V. *Chem. Mater.* **2003**, *15*, 3643.
(15) Rajić, N.; Arčon, I.; Kaučič, V.; Kodre, A. *Croat. Chem. Acta* **1999**, *72*, 645.
(16) Rajić, N.; Ristić, A.; Kaučič, V. *Zeolites* **1996**, *17*, 304.
(17) Tong, Y. *J. Magn. Reson., Ser. A* **1996**, *119*, 22.
(18) Massiot, D.; Farnan, I.; Gautier, N.; Trumeau, D.; Trokiner, A.; Coutures, J. P. *Solid State Nucl. Magn. Reson.* **1995**, *4*, 241.
(19) Sandreczki, T.; Ondercin, D.; Kreilick, R. W. *J. Magn. Reson.* **1979**, *34*, 171.
(20) Nayeem, A.; Yesinowski, J. P. *J. Chem. Phys.* **1988**, *89*, 4600.
(21) Simmen, A. Ph.D. Thesis No. 9710, ETH Zürich, 1992.
(22) Tuel, A.; Caldarelli, S.; Meden, A.; McCusker, L. B.; Baerlocher, Ch.; Ristić, A.; Rajić, N.; Mali, G.; Kaučič, V. *J. Phys. Chem. B* **2000**, *104*, 5697.
(23) Arieli, D.; Vaughan, D. E. W.; Strohmaier, K. G.; Thomann, H.; Bernardo, M.; Goldfarb, D. *Magn. Reson. Chem.* **1999**, *37*, S43.
(24) Escobal, J.; Pizarro, J. L.; Mesa, J. L.; Lezama, L.; Olazcuaga, R.; Arriourtua, M. I.; Rojo, T. *Chem. Mater.* **2000**, *12*, 376.